Journal of Hazardous Materials, 19 (1988) 51–68
Elsevier Science Publishers B.V., Amsterdam — Printed in The Netherlands

WATER CONTENT AND ENERGY BALANCE FOR GAS CLOUD EMANATING FROM A CRYOGENIC SPILL

M. RUFF, F. ZUMSTEG and T.K. FANNELØP

Departement of Mechanical Engineering, Swiss Federal Institute of Technology, CH-8092 Zurich (Switzerland)

(Received November 11, 1987; accepted March 9, 1988)

Summary

The source processes associated with the evaporation and initial spreading of cryogenic gases on water are investigated in a laboratory experiment. The direct contact of liquid nitrogen and water gives rise to phenomena which exert strong influence on the driving potential of the cold gas cloud; here investigated are superheating, and single and two-phase mass and energy transfer. Certain quantities have been measured directly in the source region or in the insulated spreading channel; others have been inferred from mass and energy balances. The water content in the cloud outside the source region, is found to consist only of ice particles; their size and number density have been determined by laser diffraction spectrometry.

Introduction

As better methods to predict the spread and dilution of heavy gas clouds are being developed, it becomes increasingly important to define the source conditions accurately, i.e. to give reliable estimates of the amount, concentration and the thermodynamic state of the gas at the source. The problem of defining the source conditions is perhaps as difficult as the dispersion problem itself, but it lends itself better to laboratory investigations.

Cryogenic spills represent one type of source where the initial conditions required in the dispersion analysis are very difficult to define even when the amount spilled and the environmental conditions are given. The rate of gas produced will first of all be dependent on the area of the cryogenic liquid layer. Experimental results on its rate of spread on water are known from the work of Chang and Reid [1], and Webber and Brighton [2] have recently developed solutions for the spreading both on water and solid surfaces. Boyle and Kneebone [3] investigated the spill of LNG on water and reported heat fluxes during the evaporation phase about 10% lower than we have measured with liquefied nitrogen over still water.

Less is known about the complicated two-phase processes associated with

0304-3894/88/$03.50

the actual evaporation of a cryogenic gas on water. It is a common experience that the temperature measured in the cloud near the water surface is considerably higher than the boiling temperature of the liquid gas; this is called superheat. The spreading rate of the cloud is proportional to the square root of the density difference between gas and air. When corrected for superheat and the latent heat of the water pick-up, this difference is much reduced, perhaps by thirty to forty percent.

High rates of mass transfer are found both in the pool boiling area and in the area where the cold gas comes into direct contact with the warm water surface. The condensation and freezing of the water transferred to the cloud have been found by Colenbrander and Puttock [4] to be major contributors to the energy balance.

The boiling of the liquefied gas could lead to droplet formation due to mechanical processes, such as bubble collapse or droplet breakup, but such phenomena were not observed. Emblem, Krogstad and Fanneløp [5] referred to such processes to explain discrepancies in the overall heat balance of cold clouds. Poag [6] in a recent dissertation has studied the mass transfer process from a wet spreading surface. The evaporation was arranged so as to give no direct contact between the liquid gas and the water, but the cloud outside the evaporation zone was allowed to spread over open water. Mass transfer in agreement with a theoretically ,determined diffusion flux across the boundary layer was observed. Colenbrander and Puttock's experiment produced both types of mass transfer, as liquefied nitrogen first evaporated with direct liquid-to-liquid contact, and the cloud thereupon spread over an open water surface. They measured an increase in the water content of the cloud with the length of travel over the open water surface. Their measured water content after evaporation is much lower than the values found in our experiment; typically they found 0.4% in terms of water to gas mass fraction whereas we found 1.5%.

In the experiment described here, liquefied nitrogen evaporated in direct contact with water, but the subsequent spreading took place over an insulated dry surface. It was a steady-state experiment, and unlike the unsteady releases of Emblem et al., there is no doubt that the low conductivity spreading surface really was dry. The scale of the present experiment is larger than that of Colenbrander and Puttock, by a factor of five in linear dimensions and about three in the specific gas flow rate. The scale is small, however, in comparison with a full-scale spill and the entrainment rates observed are, therefore, perhaps not comparable. But a steady flow experiment on this smaller scale can nevertheless produce data that are also of interest for real spills. In addition, the well-defined flow environment produced in the present setup has allowed tests and checks on methods and instruments intended for use in larger-scale instantaneous spills.

The film boiling processes are believed to be largely unaffected by scale for reasonably large heat transfer surfaces (present size, about 0.25 m^2); likewise

unaffected by scale are the superheat, the size distribution of the water droplets produced and the rate of cooling of the bulk water. In the present experiment, with temperature differences up to $\Delta T = 210$ K, the liquid nitrogen evaporation always occurred as film boiling [8]. By means of a specially designed setup, this boiling phenomenon was investigated in more detail. It was found that a very thin sheet of ice separated the LN_2-layer and the water surface, in the absence of forced mixing by mechanical means. This ice melted almost immediately after the LN_2 had evaporated. Without a determined effort to observe the interface during the evaporating process, the presence of an ice layer would not have been suspected.

The fog which blocks the view of the evaporating layer consists of water droplets or ice particles of unknown size and number density distribution. Droplets of a wide range of sizes could lead to stratification in the cloud and to energy transfer as heavy particles settle on the ground. The condensation, freezing and subsequent melting of water particles also affect the cloud density and thereby its range and rate of spreading. We have attempted to quantify these influences in various ways: by direct measurements of the water content in the cloud using gas samplers, by measuring the mass loss in the bulk water, by direct measurement of the particle size distribution using laser diffraction spectrometry, and indirectly by calculating the energy balances, making use of the detailed temperature and velocity measurements.

The volumetric flow rate of the moving cloud can be determined from the measured evaporation rate, the deduced air entrainment rate and the cloud height as determined from the temperature records. The average cloud velocity determined in this manner can in turn be compared with results of the direct velocity measurements. This comparison is of interest because the velocity instruments available were not intended for this type of measurement of very low velocities and extremely low temperatures. Calibration facilities suitable for this problem are not known to be available at present.

In what follows we shall describe the experimental setup, the instrumentation and the methods of measurement. The discussion of the results obtained emphasizes the energy balances and how these can be used to ascertain consistency and verification of the independent measurements.

Experimental arrangement and instrumentation

Our recent experiment with large unsteady releases of liquefied nitrogen, evaporating on water and spreading over a dry insulated surface, indicated an unexpectedly rapid heating of the cloud (Zumsteg and Fanneløp [7]). The gas samplers used gave much higher water contents than those found by Colenbrander and Puttock [4] in a steady cloud after evaporation. We were led to believe that phase-change processes in the spreading cloud could be important in spite of the dry laboratory atmosphere and the dry spreading surface. Em-

blem et al. [5] also found that phase change is important, in an analogous experiment, but the spreading surface used – styrofoam plates floating on a water bed intended to ensure a level surface – was perhaps not dry. It was observed that the floating plates became waterlogged during the course of the experiment, which could affect both heat and mass transfer. In view of this somewhat contradictory information, we decided to undertake a steady-state experiment which allows more detailed measurements than is possible in an instantaneous release.

To reproduce the evaporation phenomena found in the unsteady release, a large water basin was chosen ($2 \times 1.75 \times 0.15$ m) so there would be little change in water temperature during the experiment (typical run time and temperature change 10 min and 2 K). The actual evaporation surface was much smaller (0.52×0.52 m), which reduced the LN_2 flow rate required to produce a continuous layer on the water surface. The evaporation took place in an insulated enclosure with a rather small outlet to prevent air entrainment at the source. The flow of cold gas was directed onto a horizontal channel of length 5 m and width 0.5 m, built from insulating polystyrol foam plates with a smooth surface (Fig. 1). The passage time along the length of the channel was about 10 seconds, i.e. it was short in comparison with the run time. The times required to cool the channel surface and to establish a steady evaporation rate, were much longer, but after 5 minutes steady conditions were always achieved (Fig. 2). Liquefied nitrogen was supplied from a bottle, pressurized by helium at 0.5 bar through a copper pipe with its outlet in the center of the evaporation area, 15 cm above the water surface. The flow rate of approximately 3 l min^{-1} of LN_2 was monitored continuously by weighing the bottle and its content on a high-accuracy balance. Four fixed stations, which were used for the temperature, water content and velocity measurements, were located at $x=0$, 1.5, 3.0 and, dependent on the experiment, at 4.2 m, 4.3 m or 4.5 m from the beginning of the channel (Fig. 1).

The instrumentation consisted of 8 rapid response ($\tau < 0.1$ s) thermocouples to measure the cloud temperature, 5 gas samplers to determine the water content in the cloud, and 3 platinum temperature sensors to monitor the water temperature. In addition, embedded temperature sensors at various depths in the channel floor were used to determine heat transfer rates and to assure steady conditions. Continuous measurement of the conditions in the laboratory, showed these to be very stable at $T_a = 296$ K, $p_a = 0.96$ bar and relative humidity 28%.

The rapid response thermocouples and the gas samplers have been developed at our Institute and are described by Zumsteg and Fanneløp [7]. The other instruments used are state-of-the-art commercial equipment. Instrumentation suitable for accurate velocity measurement for the conditions of interest is not readily found. To check on its suitability for the larger unsteady releases, we tried a Schiltknecht propeller anemometer of external diameter

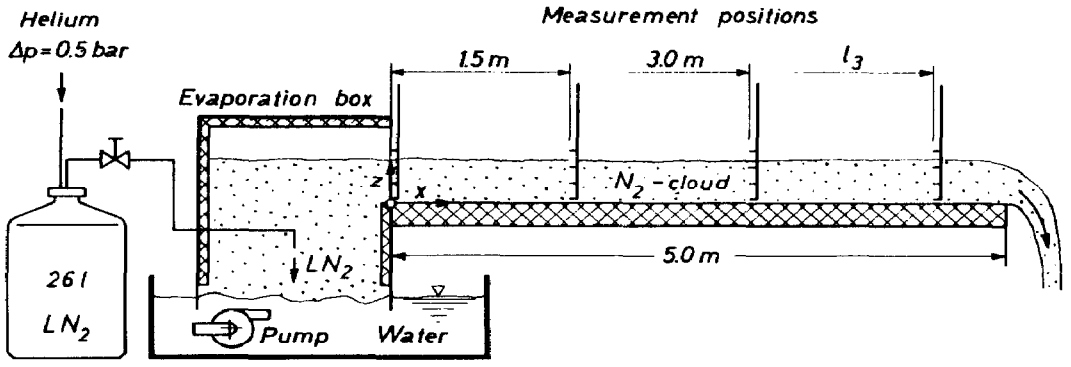

Fig. 1. Experimental setup (not to scale).

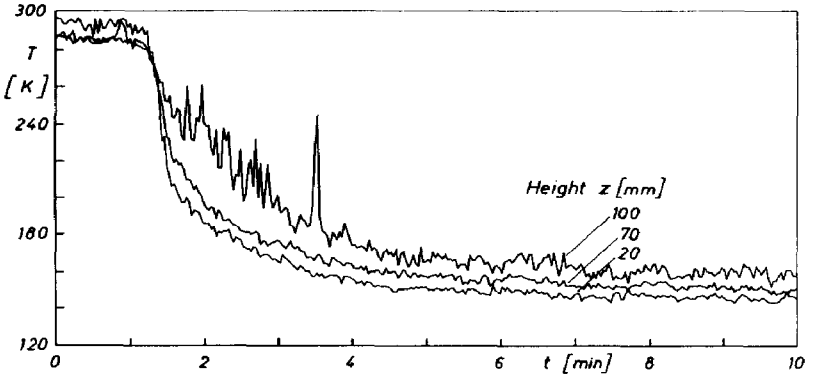

Fig. 2. Typical temperature traces at the box outlet.

20 mm. Although guaranteed only down to a temperature of 263 K we measured velocities at temperatures as low as 190 K but after about 20 seconds of continuous use the propeller became blocked by ice. The accuracy and validity of these velocity measurements can be checked from the overall mass flow balances, as discussed in a later section.

The cloud, with the appearance of a white fog, consisted of cold gas, nitrogen and air, and a small amount of water in the form of ice particles or water droplets. The water content was determined by heating the gas collected in the samplers to a temperature above the dew point, usually to 300 K. The relative humidity of the sample was measured and this revealed the total water content. But this measurement alone gave no information about the type of particles, their size or number density. To deduce the particle size distribution we used a 5 mW helium–neon laser Fraunhofer diffraction spectrometer. A cloud sample, generated by evaporating LN_2 on water, was produced in the neighborhood of the apparatus and directed through the observation volume. The particles were found to be small which, at these low temperatures and long residence time, means that they have to be ice particles.

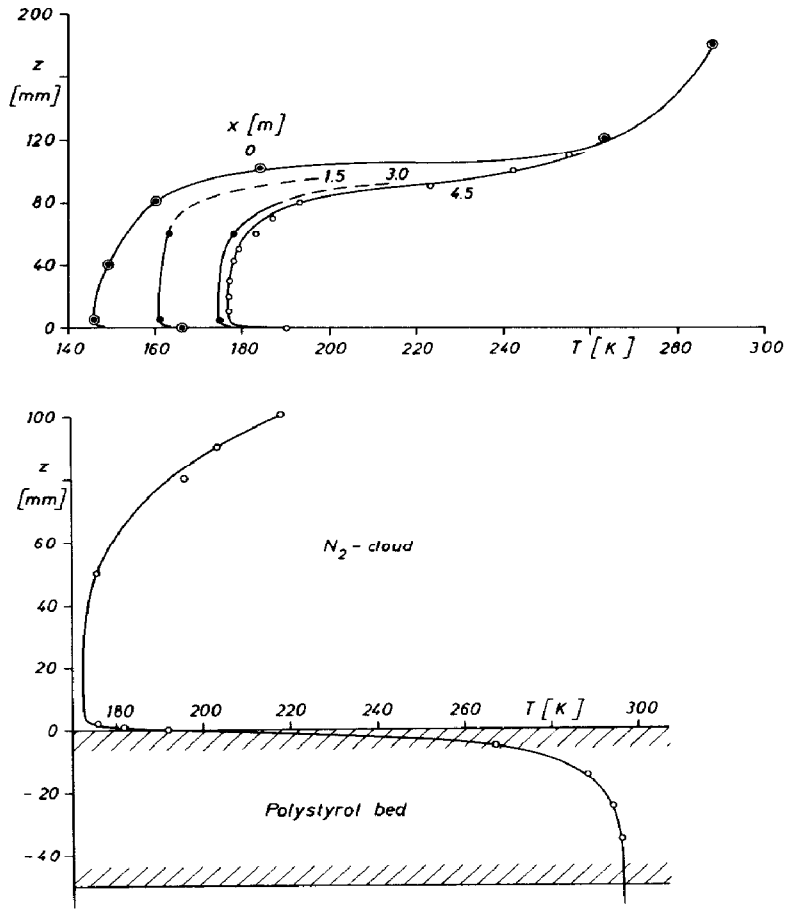

Fig. 3. Temperature profiles: (top) for Run 1 at different downstream locations; (bottom) in cloud and channel bed at $x = 2.6$ m and $t = 254$ s.

As a further check on the amount of water in the cloud, a separate experiment was undertaken, with a smaller pan (25 l of water and 0.45×0.45 m evaporation area), to measure directly the loss of bulk water during the evaporation process. The water loss, as determined by weighing the pan and content during the evaporation, should agree with the measured flow of water in the cloud as determined by the samplers. The two methods produced results in satisfactory agreement as discussed in the following section.

Discussion of results

We shall first discuss the results of the direct measurements and thereafter the results obtained indirectly from the mass and energy balances. By a series of measurements of temperature and velocity across the channel, the two di-

mensional character of the flow was verified. Subsequent measurements were performed only along the centerline.

Temperature measurements

Typical temperature profiles both in the cloud and in the polystyrol bed below are shown in Fig. 3a and b. The boundary layer along the floor and the mixing layer above may be clearly recognized. The temperature in between is seen to be approximately constant, indicating that the cloud is well mixed. The profile of the shear layer, separating the cold nitrogen gas in the cloud from the stationary air above, appears to follow a Gaussian distribution quite well. The inflection point of the fitted curve is used here as a measure of cloud thickness, it corresponds very closely with the visible height at all stations.

The gas in the evaporation box had a temperature much higher than the boiling temperature of nitrogen; the lowest temperature measured was 123 K. This measured superheat of 46 K is confirmed also by the heat balance.

Velocity measurement

The only station at which velocity profiles have been measured is $l_3 = 4.3$ m (Fig. 4). (Further upstream the temperatures were too low for the anemometer.) It is apparent that the shear layer at the top of the gas cloud and the boundary layer along the floor are smeared by the poor resolution. The probe diameter is about 20% of the cloud height, and much larger than the boundary layer thickness. The velocity profile in the shear layer is also poorly reproduced and it could not be measured in its entirety, since the minimum velocity of the instrument is 0.3 m s^{-1}.

The Reynolds number of the flow reaches the critical range only towards the end of the channel ($Re_{l_3} = (0.6 \times 4.3)/(5.86 \times 10^{-6}) = 4.4 \times 10^5$), therefore we expect the boundary layer along the channel to be mostly laminar. From the

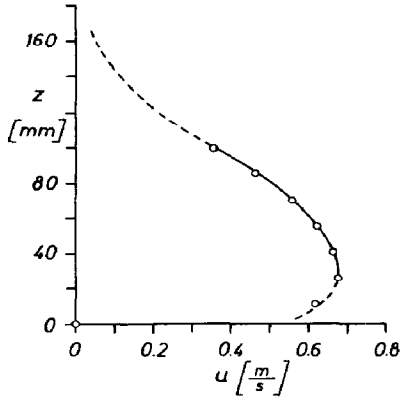

Fig. 4. Velocity profile, Run 3, $x = 4.3$ m.

various measurements, the cloud itself appears to be well mixed, i.e. here we have turbulent flow. The Prandtl number in the cold layer is near unity ($Pr=0.72$) so that the velocity and the normalized temperature profiles should in either case be similar. Although the detailed velocity profile from the propeller anemometer has obvious deficiencies, the integrated mass flux was found to be in good agreement with the calculated value. This indicates that the instrument can be useful for bulk velocity measurements on a larger scale where its diameter is small relative to the cloud height.

Water content

The gas samplers gave consistent and nearly constant results for the water content over the height of the cloud and a slightly decreasing value with increasing distance from the evaporation box. This reduction in cloud humidity is a consequence of the entrainment of dry ambient air. In Run 3 an average humidity of $x_w=1.51\%$ mass fraction water to gas at the evaporation box outlet and $x_w=1.36\%$ at $l_3=4.3$ m was measured. The accuracy of these measurements is $\pm 0.04\%$. From the mass balance the required amount of entrained air α_3 can be evaluated:

$$\alpha_3=(1+\alpha_2)\cdot\frac{0.0151-0.0136}{0.0136-x_a}=0.189,$$

where $x_a=0.46\%$ is the humidity of the ambient air and $\alpha_2=0.15$ the relative mass of air entrained in the evaporation box as calculated from the heat balance. This calculation of α_3 is very sensitive to the accuracy of the humidity measurements, but it serves to confirm the results obtained from the energy balance (see next section). For a comparison of the entrainment factors α_3 from the three experiments with a slightly different channel length, it is necessary to calculate an entrainment factor per meter α_3/l_3. There was no indication, from the temperature traces, of any delayed phase change or mass transfer processes outside the evaporation box such as suggested by Emblem et al. [5]. In a stationary cloud experiment described in [7] the melting of ice was clearly recognized from the temperature traces. Due to the limited length of our channel this phenomenon was not observed.

Particle measurements

The result from the laser diffraction spectrometer measurements are given in Fig. 5 and Table 1. Figure 5 shows the volumetric distribution density q of the particles as function of their diameter d. In Table 1 the volumetric average diameter d_{50} of the particles as well as the ranges d_{10} and d_{90} are listed. In this case d_i signifies, that i percent of the total ice volume consists of particles smaller than the value listed. The setup for Run 4 and Run 5 was slightly different from the others inasmuch as the cloud had to flow through a perforated 0.8 m long Plexiglass pipe before reaching the measurement zone. This

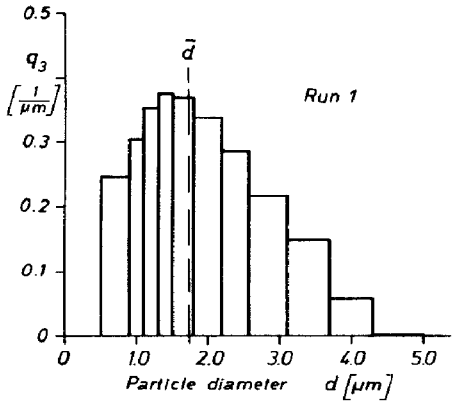

Fig. 5. Volumetric distribution density of particles in the cloud.

TABLE 1

Cloud particle diameter d (μm). d_{50} is the volumetric average diameter

Particle range	Run				
	1	2	3	4	5
d_{10}	0.47	0.48	0.48	1.49	1.70
d_{50}	1.74	1.74	1.75	2.70	2.77
d_{90}	3.23	3.16	3.15	3.93	3.93

allowed the nitrogen cloud to be mixed with ambient air and the mixing was even enhanced by the suction from a vacuum pump. But the main result obtained is common for all tests, i.e. the particles generated are all very small, 90% are less than $d = 4$ μm. Together with the actual low temperature this leads to the conclusion that the water content must be in the form of ice. When this information is combined with the known content per unit volume, we arrive at a particle number density between 10^{10} and 10^{11} per liter gas. Although the sample analyzed was generated from a small-scale evaporation of LN_2 on water, ice particle sizes in this range have also been observed on a metereological scale, as a result of spontaneous freezing of liquid water in a cold environment [9,10,11]. This spontaneous freezing is due to a known fundamental phenomenon, that below the critical temperature of 233 K a homogeneous nucleation transforms all liquid water drops to ice particles. With the small particle sizes found, gravity stratification in the cloud due to the particles will not occur. The fall velocity for an average size particle $\bar{d} = 1.79$ μm, is as low as 0.16 mm s^{-1}. Relative to the effects of temperature differences, the water contribution to the cloud density is negligible. The phase change processes (droplet formation

and freezing) on the other hand, increase the cloud temperature and contribute significantly to its reduction in density and thereby to the rate of spreading.

The normalized mass loss of water during the evaporation in the present experiments was approximately 1.6% mass fraction water to LN_2, but it appears to be dependent on the rate of nitrogen supply, on whether the water is stirred or not (which affects the ice formation on the water surface), and on the water temperature and purity in ways which are not yet understood. The rate of ice formation depends also on the size of the pan relative to the LN_2 flow rate.

Balances for mass and energy

By means of mass and energy balances it becomes possible to infer important results which cannot be measured directly with the instrumentation available.

The heat balance for the evaporation box (the enclosure defined in Fig. 6) is important because it provides information concerning superheat, i.e. it explains why the gas produced by the evaporation process has a considerably higher temperature than the known boiling point for the gas. The detailed energy balance for the evaporation process is given in the Appendix. It is used also to evaluate the unknown air entrainment $\alpha_2 = \dot{m}_{air1}/\dot{m}_{LN}$ in the evaporation box. Three complete tests of about 10 minutes' duration were conducted.

The values quoted in the sample analysis discussed in what follows refer to Run 3. In the steady-state the LN_2 flow rate was measured to be $\dot{m}_{LN} = 0.035$ kg $s^{-1} \pm 1\%$. The loss of heat from the water basin is given by $\dot{Q} = m_w c_w (\Delta T / \Delta t)$ where the water mass $m_w = 460.2$ kg and the specific heat capacity $c_w = 4.186$ kJ kg^{-1} K^{-1}. The heat per unit mass of nitrogen flowing from the water becomes $q = \dot{Q}/\dot{m}_{LN} = 242.1$ kJ $kg^{-1} \pm 3\%$. The drop in water temperature during this experiment was measured to be $\Delta T = 2.46$ K. From an estimate of the wall

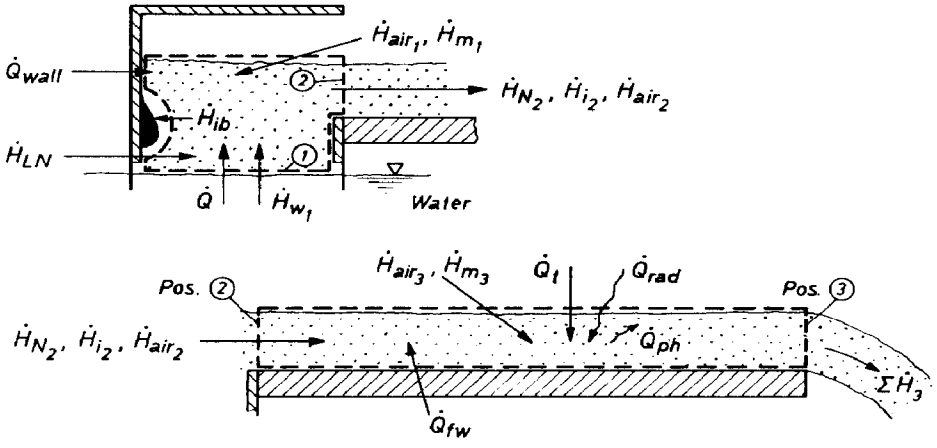

Fig. 6. Enthalpy flows: (top) in the evaporation box; (bottom) in the channel.

heat transfer the inflow to the evaporation box is determined to be $q_{wall}=\dot{Q}_{wall}/\dot{m}_{LN}=5.71$ kJ kg^{-1}. After each run an ice layer remained on the interior wall of the evaporation box and by weighing it was found to be $\Delta m_{ib}=0.142$ kg. Thus $x_{ib}=\Delta m_{ib}/(\Delta t\cdot\dot{m}_{LN})=0.72\%$ time averaged loss rate of water due to wall icing. The ice layer temperature evaluated by a heat transfer calculation is also estimated: $T_{ib}=179$ K. To obtain the average cloud temperature at the outlet of the box (Pos. 2), a reproducible height is defined by the position of the inflection point in the temperature profile, since no concentration was measured. This could lead to errors in the estimate of the air entrainment, but the analogy between heat and mass transfer for a Schmidt number close to unity in steady flow, indicate that the difference will be small. The inflection point for the temperature profile can differ somewhat from that of the concentration profile, due to latent heat release. The corresponding shift is estimated to be of the order of $\Delta z=+2$ mm as calculated from energy considerations, taking into account only the water entrained with the ambient air in the evaporation box.

The spontaneous freezing of the water pick-up from the surface has no influence on the position of the inflection point. The freezing of the entrained water during the spreading along the channel, releases heat which could tend to invalidate the analysis. But our observations show that freezing occurred only very close to the water surface.

In Run 3 the average steady-state temperature at the evaporation box outlet was $T=157.8$ K. At the same station the gas samplers measured a uniform humidity of $x_2=1.51\%$ mass fraction water to gas, where the gas was a specific mixture of nitrogen and air. The water content relative to $\dot{m}_{LN}$ can be written:

$$x_{i_2}=(1+\alpha_2)x_2.$$

Here the entire phase transition is included. This expression, together with equation (1) in the Appendix, determine α_2 and x_{i_2} through iteration. We found $\alpha_2=0.15$ kg$_{air}$/kg$_{LN}\pm 15\%$. Based on this result, the influence of the different heating effects in the evaporation box can now be discussed.

It is clear that the major source of heat is the bulk water. The temperature rise of $\Delta T=80.9$ K from the boiling temperature T_B of nitrogen to the average outlet temperature T_2 is the sum of the following values: 41 K due to heating from bulk water, 22 K due to air entrainment, 9 K due to latent heat released from the water in the cloud, 5 K due to conduction through the walls and 4 K due to ice formation on the interior wall. The lowest temperature that can be measured directly over the liquid nitrogen layer depends on how fast the water content in the cloud freezes. With the assumption of instantaneous freezing, the superheat, defined as the difference between the lowest cloud temperature and the boiling temperature of LN_2, becomes $\Delta T_{sh}=50$ K, including the contributions from heating from the bulk water and latent heat release. The measured value is only 4 K lower. A cloud from a large-scale spill (e.g. LNG on

water) also experiences a temperature rise due to heating from the water and from latent heat release as well as from air entrainment during the evaporation process. These cold clouds are therefore less hazardous than assumed in a conservative spreading analysis, where the initial cloud temperature is set equal to the gas boiling temperature. Significant heating of the cloud in the source region appears to be the rule for any spill of cryogenic fluids on water.

The discussion above refers specially to Run 3, but Table 2a lists the results of all three complete test runs. It should be noted that the water pump location in the evaporation pan was changed between each run. The intensity of stirring appears to be of some importance both for the evaporation and heating processes.

The overall energy balance for the cold gas flow spreading along the channel, provides information on the rate of air entrainment and on the relative influences of the different heating effects.

The energy balance used to evaluate the unknown amount of air entrained $\alpha_3 = \dot{m}_{air_3}/\dot{m}_{LN}$ is given in the Appendix as equation (2) (cf. Fig. 6b).

To determine the heat flow through the floor and the walls of the channel $\dot{Q}_{fw}$, the measured temperature profile in the channel bed (Fig. 3b) was used. From the given material properties the heat flow was found to be 257 W for a length of $l_3 = 4.3$ m. The heat flow from the ambient air into the top of the nitrogen cloud $\dot{Q}_t$, was calculated in three different ways; by a Reynolds-analogy estimate, by a heat conduction analysis using the measured temperature gradient at the top of the cloud, and by an integration of the heat defect as

TABLE 2

Results of the global energy balances:
(a) for the evaporation box, where: $\dot{Q}$: heat flow from bulk water into the cloud; $x_{2_{meas}}$: measured cloud humidity at Pos. 2; ΔT_{ph}: temperature rise due to phase transition of water droplets; and ΔT_{bw}: temperature rise due to heat transfer from bulk water.
(b) For the channel, where: $\Sigma\dot{Q}$: sum of heat flows into the cloud; and β: air entrainment rate based on the average velocity at Pos. 3

(a) Run	x_a kg_w/kg_{air}	$\dot{m}_{LN}$ kg/s	$\dot{Q}$ W	T_2 K	$x_{2_{meas}}$ kg_w/kg_{gas}	α_2 kg_{air}/kg_N	ΔT_{ph} K	ΔT_{bw} K
1	0.0044	0.0406	9947.8	156.1	0.0144	0.123	8.5	43.7
2	0.0043	0.0396	9242.8	150.1	0.0133	0.155	8.0	32.5
3	0.0046	0.0352	8523.3	157.8	0.0151	0.147	9.0	40.8

(b) Run	$\Sigma\dot{Q}$ W	T_2 K	T_3 K	α_3/l_3 $kg_{air}/(kg_N \cdot m)$	β —	l_3 m
1	602	156.1	183.6	0.0312	0.0034	4.5
2	523	150.1	175.6	0.0316	0.0037	4.2
3	535	157.8	182.0	0.0256	0.0028	4.3

given by the measured temperature profiles. In all methods the height of interest ranged from the inflection point (defined as cloud height h_c) to a large height at which the ambient temperature prevailed. For all these methods we obtained consistent values of about $\dot{Q}_t = 191$ W for the length $l_3 = 4.3$ m. The total heat transferred to the cloud was $\sum \dot{Q} = 535.1$ W $\pm 20\%$ where the effect of radiation from the environment, $\dot{Q}_{rad} = 87$ W, also is included. The average temperature of the cloud rose from $T_2 = 157.6$ K at the beginning of the channel to $T_3 = 182.8$ K at its end. Based on the cloud humidity, $x_2 = 1.5\%$, the mass fraction water to gas, at the evaporation box outlet, the amount of entrained air $\dot{m}_{air_3}/\dot{m}_{LN}$ during the passage along the channel is found to be: $\alpha_3 = 0.12$ $kg_{air}/kg_{LN} \pm 20\%$. This leads for the three runs to an air entrainment rate per unit length of $\alpha_3/l_3 = 0.031$ m^{-1}, 0.032 m^{-1} and 0.026 m^{-1}. Colenbrander and Puttock [4] measured an air entrainment rate of approximately $\alpha = 0.04$ m^{-1}, which is 25% higher than our maximum value. The heat difference could perhaps be attributed to the higher heat flux from below in [4], in which case the nitrogen gas cloud was developing over a constant temperature water surface.

Another form of the entrainment rate often used, is defined by the velocity ratio $\beta = w_e/u_3$, where w_e is the vertical entrainment velocity. β can be calculated from the known α values:

$$\beta \approx \gamma \frac{h_c \bar{\rho}}{l_3 \rho_a} \cdot \frac{\alpha_3}{1 + \alpha_2 + \alpha_3},$$

where $\gamma = 0.97$ is a correction for the sidewall boundary layer displacement and l_3 the length on which α_3 is based. For the three runs the values $\beta = 0.34\%$, 0.37% and 0.28% are found. Entrainment data from the experiments of Poag [6] are of the order of $\beta = 1\%$ and are therefore significantly higher. A possible explanation is that his nitrogen cloud evaporated dry over a warmed aluminum foil with a constant temperature of 300 K and was subsequently allowed to spread over open water. This led to heating rates from the floor three times higher than in our case.

From the known mass flow of nitrogen and the calculated entrained air, the total mass flow at the end of the channel is found. This allows checks both on the accuracy of the propeller anemometer and our energy balance. No direct method is available to us for calibration of this anemometer at the low velocities (< 1 m s^{-1}) and extreme temperatures (down to 123 K) of interest. For Run 3 the mass flow was found from the mass balance to be

$$\dot{m}_3 = \dot{m}_{LN}(1 + \alpha_2 + \alpha_3) = 0.044 \text{ kg s}^{-1}$$

and the integrated mass flow as determined from the measured velocity and temperature profiles gave $\dot{m}_3 = \int_0^{h_c} \rho u \, dz = 0.046$ kg s^{-1}. The calculated mass flow from the energy balance is 3.5% smaller. The anemometer is a displacement

flow device, but in regions of large gradients it responds also to dynamic pressure. For this reason it records too high values in boundary and shear layers. But the overall accuracy of the propeller anemometer for the difficult flow conditions is encouraging.

Conclusions

Detailed experiments of the steady evaporation and spreading of cold gas clouds emanating from liquid nitrogen spills on water, have been undertaken. The instrumentation used includes thermocouples, gas samplers in combination with a relative humidity sensor and a propeller anemometer. These instruments have been found to be adequate for the experiments and to give data which are consistent and of reasonable accuracy. It is found that the evaporation process, liquefied nitrogen on water, leads to initial cloud temperatures significantly above the gas boiling point. This reduces the driving potential of the cloud and in turn leads to reduced hazard potential in comparison with the conservative assumption that the boiling temperature represents the initial source condition. The main causes for the heating are heat transfer from the water and the latent heat release of water picked up by the cloud. The cloud water content in the source region is approximately $x_2 = 1.5\%$ (mass fraction, water to gas), which together with the heat transfer represent a temperature rise of about 50 K.

As the cloud spreads along the channel with its insulated floor, air entrainment rates of $\alpha_3/l_3 = 0.03$ (increase in mass fraction per meter), or alternatively $\beta = 0.0033$ (entrainment to mean flow velocity ratio) are found. Even at this low level of mass transfer, the air entrainment is found to be the most important effect in heating the cloud, about equal to all other influences combined.

The water picked up in the evaporation process forms particles of size 2–4 μm. For such small particles no stratification in the cloud is expected. At the very low temperatures found, spontaneous phase transition to ice occurs. No other mass transfer process of consequence is possible before the cloud reaches the temperature where the ice begins to melt.

Appendix

The evaporation box and the channel are regarded as two separate systems. Over the system boundaries the energy flows are defined and global energy balances established (cf. Fig. 6).

Assumptions

- Stationary conditions are assumed.
- Potential and kinetic energies in the cloud are neglected.

- The phase transitions of water and vapor are instantaneous.
- The amount of saturated humidity in the cold cloud is neglected.
- The heat capacities c are averaged over the actual temperature range.
- The temperatures at Pos. 2 and Pos. 3 are averaged over the height.

Evaporation box

The particular enthalpies are listed below:
Water content (due to water pick-up):
$\dot{H}_{w_1} = \dot{m}_{w_1}[c_{i_1}(273.15 - T_B) + r_s + c_w(T_w - 273.15)]$ with $T_w \approx T_a$; $c_{i_1} = 1372$ J kg^{-1} K^{-1}
Nitrogen: $\dot{H}_N = -\dot{m}_{LN}[r_N + c_{pN}(T_2 - T_B)]$
Dry air entrainment: $\dot{H}_{air} = \dot{m}_{air_1} c_{p_{air}}(T_a - T_2)$
Moisture entrainment: $\dot{H}_{m_1} = \dot{m}_{m_1}[c_{i_1}(273.15 - T_B) + r_s + r_i + c_{p_w}(T_a - 273.15)]$ with $\dot{m}_{m_1} = x_a \dot{m}_{air_1}$, and $T = 273.15$ K
Ice on box walls: $\dot{H}_{ib} = -\dot{m}_{ib} c_{ib}(T_{ib} - T_B)$ with $c_{ib} = 1061$ J kg^{-1} K^{-1}, and $T_{ib} = 150$ K
Ice in the cloud at Pos. 2: $\dot{H}_{i_2} = -\dot{m}_{i_2} c_{i_2}(T_2 - T_B)$ with $c_{i_2} = 974$ J kg^{-1} K^{-1}
Heat flow through walls: $\dot{Q}_{wall}$; estimated at 201 W
Heat flow from bulk water into cloud: $\dot{Q}$.

In the energy balance the quantities are specified by the unit mass flow of liquid nitrogen.
We therefore define:
dry air entrainment in the evaporation box: $\alpha_2 = \dot{m}_{air_1}/\dot{m}_{LN}$
for other mass fractions: $x_j = \dot{m}_j/\dot{m}_{LN}$
for specific heat: $q_j = \dot{Q}_j/\dot{m}_{LN}$
By combining the relevant enthalpy and heat flows into an energy balance, and on substituting $\dot{m}_{w_1} = \dot{m}_{i_2} + \dot{m}_{ib} - \dot{m}_{m_1}$, we can solve the equation for the unknown amount of entrained air α_2:

$$\alpha_2 = \frac{1}{c_{p_{air}}(T_2 - T_a) + x_a[(T_a - 273.15)(c_w - c_{p_w}) - r_i]} \{q + q_{wall} - r_N + (x_{ib} + x_{i_2}) \times [c_{i_1}(273.15 - T_B) + r_s + c_w(T_a - 273.15)] - [c_{pN} + x_{i_2} c_{i_2}](T_2 - T_B) - x_{ib} c_{ib}(T_{ib} - T_B)\} \quad (1)$$

where $x_{i_2} = (1 + \alpha_2) x_{2_{meas}}$. Here $x_{2_{meas}}$ is the water content measured by the gas sampler at the evaporation box outlet. This correction is required due to the increase of mass in the nitrogen cloud from entrained air.

Channel

The relevant enthalpy flows are given by:
Nitrogen in cloud: $\dot{H}_N = \dot{m}_{LN} c_{pN} (T_2 - T_3)$
Air entrained in the evaporation box: $\dot{H}_{air_2} = \dot{m}_{air_1} c_{p_{air}} (T_2 - T_3)$
Ice enthalpy: $\dot{H}_{i_3} = \dot{m}_{i_2} c_{i_5} (T_2 - T_3)$
Dry air entrainment: $\dot{H}_{air_3} = \dot{m}_{air_3} c_{p_{air}} (T_a - T_3)$
Moisture entrainment: $\dot{H}_{m_3} = \dot{m}_{m_3} [c_{i_4} (273.15 - T_3) + r_s + r_i + c_{p_w} (T_a - 273.15)]$
with $\dot{m}_{m_3} = x_a \dot{m}_{air_3}$.

Heat flows:
- at the top of the cloud: $\dot{Q}_t$; estimated at 191 W
- through floor and walls: $\dot{Q}_{fw}$; estimated at 257 W
- by radiation: $\dot{Q}_{rad}$; estimated at 87 W
- by delayed phase transition: $\dot{Q}_h = 0$.

The inflow and outflow are divided by $\dot{m}_{LN}$. With $\alpha_3 = \dot{m}_{air_3} / \dot{m}_{LN}$ and $\sum q = (\dot{Q}_t + \dot{Q}_{fw} + \dot{Q}_{rad} + \dot{Q}_{Ph}) / \dot{m}_{LN}$ we obtain

$$\alpha_3 = \frac{[\sum q + (c_{pN} + \alpha_2 c_{p_{air}} + x_{i_2} c_{i_5})(T_2 - T_3)]}{c_{p_{air}} (T_3 - T_a) + x_a [c_{i_4} (T_3 - 273.15) - r_s - r_i - c_{p_w} (T_a - 273.15)]} \tag{2}$$

Property data (Ref. 11)

Gaseous nitrogen at $p_a \approx 1$ bar:

$T_B = 77.3$ K; $R_N = 296.7$ J kg^{-1} K^{-1}; $Pr = 0.72$ $c_{pN} = 1123$ J kg^{-1} K^{-1}
at $T = T_B$; $c_{pN} = 1034$ J kg^{-1} K^{-1} at $T = 273.15$ K

Within the indicated temperatures the properties listed are described within $\pm 2\%$ by the following functions:

$r_N = 296.069 - 1.259\, T_B$ J kg^{-1} K^{-1} $70 \leq T_B \leq 80$ K

$p_B = 39095.0\, (T_B/70.0)^{9.5}$ Pa $70 \leq T_B \leq 80$ K

$\lambda = 7.57 \times 10^{-3}\, (T/T_B)^{0.93}$ W m^{-1} K^{-1} $70 \leq T_B \leq 300$ K

$\mu = 5.504 \times 10^{-6}\, (T/T_B)^{0.89}$ kg s^{-1} m^{-1} $70 \leq T_B \leq 300$ K

Liquid nitrogen:

$\rho_{LN} = 808.6$ kg m^{-3}; $c_{LN} = 2063.7$ J kg^{-1} K^{-1}

Water:

$r_s = 333$ kJ kg^{-1}; $r_i = 2501.6$ kJ kg^{-1} at $T = 273.15$ K

$c_i = 166.2 + 6.988\,T$ J kg^{-1} K^{-1}

$c_w = 4182$ J kg^{-1} K^{-1} at $T = 291$ K

$c_{pw} = 1860$ J kg^{-1} K^{-1} at $T = 293$ K

List of symbols

c	heat capacity of liquid or solid phase, J kg^{-1} K^{-1}
c_p	heat capacity at constant pressure, J kg^{-1} K^{-1}
d	particle diameter, μm
$\dot{H}$	enthalpy flow, W
h_c	height of cloud, m
m	mass, kg
p	pressure, Pa
$\dot{Q}$	heat flow, W
q	specific energy, J kg^{-1}
R	specific gas constant, J kg^{-1} K^{-1}
r_s, r_i	latent heat of evaporation and fusion, J kg^{-1}
t	time, s
T	temperature, K
x_w	water content, mass fraction
x,y,z	Cartesian coordinates
α	air entrainment factor, mass fraction
β	air entrainment factor, velocity ratio
γ	correction factor for sidewall boundary layer displacement
λ	heat conductivity, W m^{-1} K^{-1}
μ	dynamic viscosity, kg m^{-1} s^{-1}
ρ	density, kg m^{-3}

Subscripts

a	ambient
B	boiling point
bw	bulk water
fw	floor and wall of channel
i	ice
ib	ice in evaporation box
LN	liquefied nitrogen
m	moisture in ambient air
meas	measured

N	gaseous nitrogen
ph	phase transition
rad	radiation
sh	superheat
t	top
w	water
wall	wall of evaporation box
1,2,3	positions in channel

References

1 H.-R. Chang and R.C. Reid, Spreading-boiling model for instantaneous spills of liquified petroleum gas on water, J. of Hazardous Materials, 7 (1982) 19–35.

2 D.M. Webber and P.M.W. Brighton, An integral model for spreading vaporising pools, derived from shallow-layer equations, SRD Report R 340, 1985.

3 G.J. Boyle and A. Kneebone, Laboratory investigations into the characteristics of LNG spills on water: evaporation, spreading and vapor dispersion, Report to A.P.I. project on LNG spills on water, 1973.

4 G.W. Colenbrander and J.S. Puttock, Maplin sands experiments 1980. Interpretation and modelling of liquified gas spills onto the sea, in: G. Ooms and H. Tennekes (Eds.), IUTAM Symposium, Delft. Springer, 1984.

5 K. Emblem, P.Å. Krogstad and T.K. Fanneløp, Experimental and theoretical studies in heavy gas dispersion, in: G. Ooms and H. Tennekes (Eds.), IUTAM Symposium, Delft. Springer, 1984.

6 R.K. Poag, Heat transfer-induced turbulent mixing in stably stratified shear flow. Dissertation, University of Arkansas, 1987.

7 F. Zumsteg and T.K. Fanneløp, Large-scale experiments on the spreading and dilution of cold gas clouds in a controlled environment, in: E.J. List (Ed.), 3rd International Symposium on Stratified Fluids, Pasadena, 1987, California Institute of Technology Proceedings, in preparation.

8 T.M. Flynn, J.W. Draper and J.J. Roos, The nucleate and film boiling curve of liquid nitrogen at one atmosphere, Adv. Chem. Eng., 7 (1962) 539–550.

9 V.C. Schaefer, Condensed water in the free atmosphere in air colder than −40°C, J. Appl. Metereol., 1 (1962) 481–487.

10 V.C. Schaefer, The vapor method for making replicas of liquid and solid aerosols, J. Appl. Metereol., 1 (1962) 413–417.

11 R.R. Rogers, A short course in cloud physics. International Series in Natural Philosophy, Vol. 96, 2nd ed., Pergamon Press, 1979.

12 N.B. Vargaftik, Tables on the thermophysical properties of liquids and gases. 2nd ed., John Wiley, 1975.